Pairing renormalization and regularization within the local density approximation

P. J. Borycki,[1,2] J. Dobaczewski,[1,3,4,5] W. Nazarewicz,[1,3,4] and M. V. Stoitsov[1,3,5,6]
[1]*Department of Physics & Astronomy, University of Tennessee, Knoxville, Tennessee 37996, USA*
[2]*Institute of Physics, Warsaw University of Technology, ul. Koszykowa 75, PL-00-662 Warsaw, Poland*
[3]*Physics Division, Oak Ridge National Laboratory, P.O. Box 2008, Oak Ridge, Tennessee 37831, USA*
[4]*Institute of Theoretical Physics, Warsaw University, ul. Hoża 69, PL-00-681 Warsaw, Poland*
[5]*Joint Institute for Heavy-Ion Research, Oak Ridge, Tennessee 37831, USA*
[6]*Institute of Nuclear Research and Nuclear Energy, Bulgarian Academy of Sciences, Sofia-1784, Bulgaria*
(Received 18 January 2006; published 21 April 2006)

We discuss methods used in mean-field theories to treat pairing correlations within the local density approximation. Pairing renormalization and regularization procedures are compared in spherical and deformed nuclei. Both prescriptions give fairly similar results, although the theoretical motivation, simplicity, and stability of the regularization procedure make it a method of choice for future applications.

DOI: 10.1103/PhysRevC.73.044319 PACS number(s): 21.60.Jz, 31.15.Ew, 21.10.Dr

I. INTRODUCTION

One of the main goals of low energy nuclear theory is to build a comprehensive microscopic framework in which nuclear bulk properties, excitations, and low energy reactions can be described. For medium-mass and heavy nuclei, self-consistent methods based on the density functional theory (DFT) [1,2] have already achieved a level of precision that allows for analysis of experimental data for a wide range of properties of nuclei throughout the nuclide chart. For example, the self-consistent Hartree-Fock-Bogoliubov (HFB) models based on the Skyrme energy functionals [3–5] can reproduce nuclear masses with an rms error of about 700 keV [6,7]. The development of a universal nuclear density functional, however, still requires a better understanding and improved description of density dependence, isospin effects, pairing force, many-body correlations, and symmetry restoration.

Nuclear pairing is an important ingredient of the nuclear density functional, and it becomes crucial for open shell nuclei, in particular weakly bound systems, where the effects of coupling to continuum become significant [8,9]. In this case, the BCS model is not adequate [8] and the fully self-consistent HFB approach must be used.

In most HFB applications, pairing interaction is assumed to be either in the form of the finite-range Gogny force [10] or the zero-range, possibly density-dependent, delta force [8,9,11]. Gogny interaction in the pairing channel can be viewed as a regularized contact interaction, with regularization fixed through the finite range. The resulting pairing field is, however, nonlocal.

Calculations using the contact interaction are numerically simpler, but one has to apply a cutoff procedure within a given space of single-particle (s.p.) states [8,12]. When the dimension of this space increases, the pairing gap diverges for any given strength of the interaction. Therefore, the pairing strength has to be readjusted for each s.p. space. Thus, the energy cutoff and pairing strength together define the pairing interaction, and this definition can be understood as a phenomenological introduction of finite range [8,13]. Such a procedure is usually referred to as the renormalization of the contact pairing force. It is performed in the spirit of the effective field theory, whereupon contact interactions are used to describe low energy phenomena while the coupling constants are readjusted for any given energy cutoff to take into account neglected high energy effects.

The renormalization procedure for the zero-range pairing interactions has been explored in Ref. [8] using the numerical solutions of the HFB equations. It has been shown that by renormalizing the pairing strength for each value of the cutoff energy one practically eliminates the dependence of the HFB energy on the cutoff parameter.

Recently, the issue of contact pairing force has been addressed in Refs. [14–23], suggesting that the renormalization procedure can be replaced by a regularization scheme which removes the cutoff energy dependence of the pairing strength. In particular, pairing regularization has been applied to properties of infinite nuclear matter [19], spherical nuclei [21,23,24], and trapped fermionic atoms [16,25]. Different pairing schemes and regularization recipes were discussed in Ref. [23].

In this study, we investigate the stability of the regularization scheme with respect to the cutoff energy for both spherical and deformed nuclei. Differences between the HFB results emerging from the pairing renormalization and pairing regularization procedures are analyzed.

The HFB and Skyrme HFB formalisms have been explained in great detail in many papers (see, e.g., Refs. [12,26]). The notation used in the present paper is consistent with that of Refs. [8,12,27]. This work is organized as follows. Section II gives a brief introduction to the pairing renormalization and regularization schemes. In Sec. III, we explain the numerical framework used. The comparison between pairing regularization and renormalization techniques, studied for a large set of spherical and deformed nuclei, is discussed in Sec. IV. Finally, the summary and conclusions are given in Sec. V.

II. CUTOFF PROCEDURES

A. Pairing renormalization procedure

Within the HFB theory, the energy cutoff can be applied to either the s.p. or the quasiparticle spectrum. The first option is used when the HFB equations are solved within a restricted s.p. space. However, the s.p. energies play only an auxiliary role in the HFB method, and the cutoff applied to the quasiparticle spectrum is more justified. This is done by using the so-called equivalent s.p. spectrum [12]

$$\bar{e}_n = (1 - 2P_n)E_n + \mu, \tag{2.1}$$

where E_n is the quasiparticle energy and P_n denotes the norm of the lower component of the HFB wave function.

Because of the similarity between $\bar{e}_n$ and the s.p. energies, one takes into account only those quasiparticle states for which $\bar{e}_n$ is less than the assumed cutoff energy $\epsilon_{\rm cut}$.

It was shown [8] that for a fixed pairing strength the pairing energies depend significantly on the energy cutoff. Within the renormalization scheme employed in this work, we use the prescription of adjusting the pairing strength to obtain a fixed average neutron pairing gap [12],

$$\bar{\Delta} = -\frac{1}{N}\int d^3\mathbf{r}d^3\mathbf{r}' \sum_{\sigma\sigma'} \tilde{h}(\mathbf{r}\sigma, \mathbf{r}'\sigma')\rho(\mathbf{r}'\sigma', \mathbf{r}\sigma), \tag{2.2}$$

in ^{120}Sn equal to the experimental value of 1.245 MeV. In Eq. (2.2), N is the number of particles, ρ is the particle density, and $\tilde{h}$ is the pairing Hamiltonian (see the Appendix).

Such a procedure almost eliminates the dependence of the HFB energy on the cutoff [8].

B. Pairing regularization procedure

Using the HFB equations and properties of the Bogoliubov transformation (see Appendix for details), one concludes that the local abnormal density $\tilde{\rho}$ has a singular behavior when $\epsilon_{\rm cut} \to \infty$. The standard regularization technique is to remove the divergent part and define the regularized local abnormal density $\tilde{\rho}_r(\mathbf{r})$ as

$$\tilde{\rho}_r(\mathbf{r}) = \lim_{\mathbf{x}\to 0}\left[\tilde{\rho}(\mathbf{r} - \mathbf{x}/2, \mathbf{r} + \mathbf{x}/2) - f(\mathbf{r}, \mathbf{x})\right], \tag{2.3}$$

where f is a regulator which removes the divergence at $\mathbf{x} = 0$.

For cutoff energies high enough, one can explicitly identify [17–19] components generating divergence in the abnormal density [see, e.g., Eq. (21) of Ref. [18]],

$$f(\mathbf{r}, \mathbf{x}) = \frac{i\tilde{h}(\mathbf{r})M^*(\mathbf{r})k_F(\mathbf{r})}{4\pi\hbar^2} + \frac{\tilde{h}(\mathbf{r})}{2}G_\mu(\mathbf{r} + \mathbf{x}/2, \mathbf{r} - \mathbf{x}/2), \tag{2.4}$$

where G_μ is the s.p. Green's function at the Fermi level μ in the truncated space, M^* is the effective mass, and the Fermi momentum is

$$k_F(\mathbf{r}) = \frac{\sqrt{2M^*(\mathbf{r})}}{\hbar}\sqrt{\mu - U(\mathbf{r})}, \tag{2.5}$$

with U being the self-consistent mean-field potential.

The first term in Eq. (2.4) comes from the MacLaurin expansion with respect to $\mathbf{x}$; it guarantees that the regularization procedure does not introduce any constant term to the abnormal density and that $f(\mathbf{r}, \mathbf{x})$ solely represents the divergent part of $\tilde{\rho}$.

Using the Thomas-Fermi approximation, the local s.p. Green's function $G_\mu(\mathbf{r}) := G_\mu(\mathbf{r}, \mathbf{r})$ becomes [18,19]

$$G_\mu(\mathbf{r}) = \frac{1}{2\pi^2}\lim_{\gamma\to 0}\int_0^{k_{\rm cut}(\mathbf{r})} \frac{k^2 dk}{\mu - \frac{\hbar^2k^2}{2M^*(\mathbf{r})} - U(\mathbf{r}) + i\gamma}, \tag{2.6}$$

where the cutoff momentum is given by

$$k_{\rm cut}(\mathbf{r}) = \frac{\sqrt{2M^*(\mathbf{r})}}{\hbar}\sqrt{\epsilon_{\rm cut} + \mu - U(\mathbf{r})}. \tag{2.7}$$

The regularized pairing Hamiltonian and the pairing energy density may be written, respectively, as [18]

$$\tilde{h}(\mathbf{r}) = g(\mathbf{r})\tilde{\rho}_r(\mathbf{r}) = g_{\rm eff}(\mathbf{r})\tilde{\rho}(\mathbf{r}) \tag{2.8}$$

$$\mathcal{H}_{\rm pair}(\mathbf{r}) = \tfrac{1}{2}g_{\rm eff}(\mathbf{r})\tilde{\rho}(\mathbf{r})^2, \tag{2.9}$$

where the effective pairing strength [17–19],

$$g_{\rm eff}(\mathbf{r}) = \left(\frac{1}{g(\mathbf{r})} + \frac{G_\mu(\mathbf{r})}{2} + \frac{iM^*(\mathbf{r})k_F(\mathbf{r})}{4\pi\hbar^2}\right)^{-1}, \tag{2.10}$$

after calculating integral (2.6), can be expressed in the form

$$g_{\rm eff}(\mathbf{r}) = \begin{cases} \left[\dfrac{1}{g(\mathbf{r})} - \dfrac{M^*(\mathbf{r})k_{\rm cut}(\mathbf{r})}{2\pi^2\hbar^2}\left(1 - \dfrac{k_F(\mathbf{r})}{2k_{\rm cut}(\mathbf{r})}\ln\dfrac{k_{\rm cut}(\mathbf{r}) + k_F(\mathbf{r})}{k_{\rm cut}(\mathbf{r}) - k_F(\mathbf{r})}\right)\right]^{-1} & k_F(\mathbf{r})^2 \geqslant 0, \\ \left[\dfrac{1}{g(\mathbf{r})} - \dfrac{M^*(\mathbf{r})k_{\rm cut}(\mathbf{r})}{2\pi^2\hbar^2}\left(1 + \dfrac{|k_F(\mathbf{r})|}{k_{\rm cut}(\mathbf{r})}\arctan\dfrac{|k_F(\mathbf{r})|}{k_{\rm cut}(\mathbf{r})}\right)\right]^{-1} & k_F(\mathbf{r})^2 < 0. \end{cases} \tag{2.11}$$

In this regularization scheme, only Green's function is calculated using the Thomas-Fermi approximation. The densities, potentials, and chemical potential are determined self-consistently within the HFB theory. Consequently, the Fermi momentum (2.5) depends on microscopic HFB quantities. According to the sign of k_F^2, one of the expressions (2.11) is used.

In Ref. [20], a different regularization scheme has been proposed that involves truncation below and above the Fermi

level. However, the HFB calculations in the quasiparticle basis should be performed for a high cutoff energy of 50 MeV and higher [8]. Since the magnitude of the self-consistent mean-field U is also about 50 MeV, for such a high cutoff energy both methods are equivalent. The Thomas-Fermi approximation requires that in order to obtain results independent of $\epsilon_{\rm cut}$, its value should be high enough for $k_{\rm cut}$ to be real everywhere.

Through the density dependence of $g_{\rm eff}$, $k_{\rm cut}$, and k_F, there appear rearrangement terms in the self-consistent mean-field potential:

$$\frac{\delta\mathcal{H}_{\rm pair}}{\delta\rho} = \frac{\delta g_{\rm eff}}{\delta\rho}\tilde{\rho}^2 = \tilde{\rho}^2\left(\frac{\partial g_{\rm eff}}{\partial g}\frac{\delta g}{\delta\rho} + \frac{\partial g_{\rm eff}}{\partial k_F}\frac{\delta k_F}{\delta\rho} + \frac{\partial g_{\rm eff}}{\partial k_{\rm cut}}\frac{\delta k_{\rm cut}}{\delta\rho}\right). \quad (2.12)$$

The first term in Eq. (2.12) is similar to the usual rearrangement term, while the other two terms associated with the regularization procedure are entirely new. It is easy to check that all the terms appearing in Eq. (2.12) are continuous at the classical turning point $k_F(\mathbf{r}) = 0$.

In Eq. (2.9), the pairing energy density is divergent with respect to the cutoff energy. However, the pairing energy itself is not an observable, and in order for the energy density functional to be independent of the cutoff, other terms have to cancel out this divergence. As discussed in Refs. [14,15,17,18], the kinetic energy density τ has the same type of divergence as the abnormal density $\tilde{\rho}$, and the sum

$$\mathcal{H}_{\rm kin+pair}(\mathbf{r}) = -\frac{\hbar^2}{2M^*(\mathbf{r})}\tau + \frac{1}{2}g_{\rm eff}(\mathbf{r})\tilde{\rho}^2(\mathbf{r}) \quad (2.13)$$

does converge.

Various contributions to the total HFB energy as functions of the cutoff energy are shown in Fig. 1. The total energy is stable with respect to $\epsilon_{\rm cut}$, although some of the components of the total energy vary significantly. As expected from Eq. (2.13), two terms exhibiting large fluctuations are the kinetic term (with variations of about 2 MeV) and the pairing term (with variations of about 1.3 MeV). Also, the momentum-dependent spin-orbit term, $E_{\rm S.O.}$, has significant variations of about 1 MeV. On the other hand, Skyrme and Coulomb energies are fairly stable with respect to $\epsilon_{\rm cut}$.

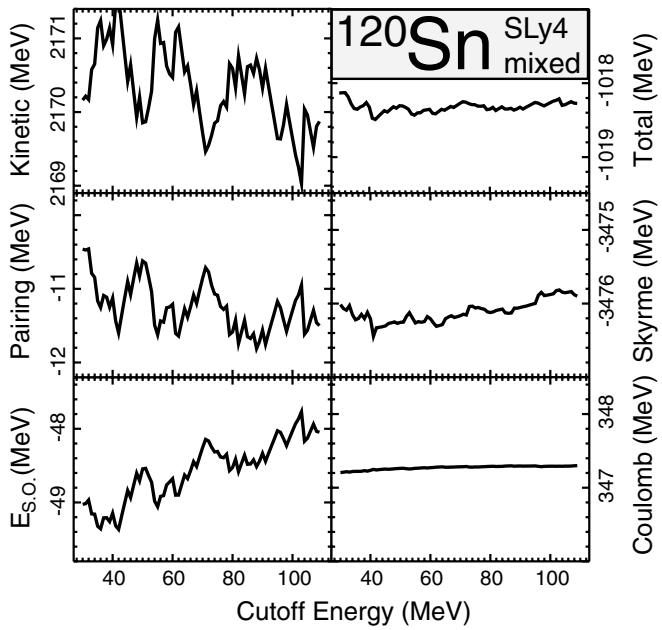

FIG. 1. Various contributions to the HFB energy for ^{120}Sn as a function of $\epsilon_{\rm cut}$. Calculations used the SLy4 Skyrme functional and mixed pairing interaction (3.1).

III. NUMERICAL IMPLEMENTATION

A. Numerical framework

As the pairing renormalization and regularization procedures remove the divergent part of the abnormal density in a different way, one can expect some numerical differences between both methods. In order to compare their results, we have performed numerical calculations using two numerical codes solving the HFB equations:

HFBRAD [28] – solves the HFB equations in the spherically symmetric coordinate basis. The maximum angular momenta used in calculations were $j_{\rm max} = 39/2$ for neutrons and $j_{\rm max} = 25/2$ for protons.

HFBTHO [27] – diagonalizes the HFB problem in the axially symmetric transformed harmonic oscillator (HO) basis. Unless stated otherwise, we use $N_{\rm osc} = 20$ HO shells in the basis.

In our calculations, we use the SLy4 [29] and SkP [12] Skyrme density functionals in the p-h channel. These parametrizations are commonly used in realistic HFB calculations. While SLy4 and SkP have rather different effective masses, this does not influence the regularization procedure as the effective mass enters the formalism explicitly, see, e.g., Eq. (2.11). In the p-p channel, we use the contact density-dependent force, which leads to the pairing energy density of the form

$$\mathcal{H}_{\rm pair}(\mathbf{r}) = \frac{1}{2}g(\mathbf{r})\tilde{\rho}(\mathbf{r})^2 = \frac{1}{2}V_0\left[1 - V_1\frac{\rho(\mathbf{r})}{\rho_0}\right]\tilde{\rho}(\mathbf{r})^2, \quad (3.1)$$

where $\rho_0 = 0.16$ fm^{-3}. For $V_1 = 0$, the resulting pairing interaction is called volume pairing, while $V_1 = 1/2$ corresponds to the so-called mixed pairing prescription (Ref. [30] and references therein).

B. Pairing renormalization

Figure 2 illustrates the importance of the pairing renormalization procedure in the case of ^{120}Sn. Due to the constraint (2.2) on the pairing strength, the neutron average pairing gap stays by definition constant, while the resulting total energy changes with the cutoff energy by a few hundred keV. On the other hand, without pairing renormalization applied, the total energy and average neutron gap vary significantly with increasing dimension of the quasiparticle space. In this case, the total energy changes by several MeV.

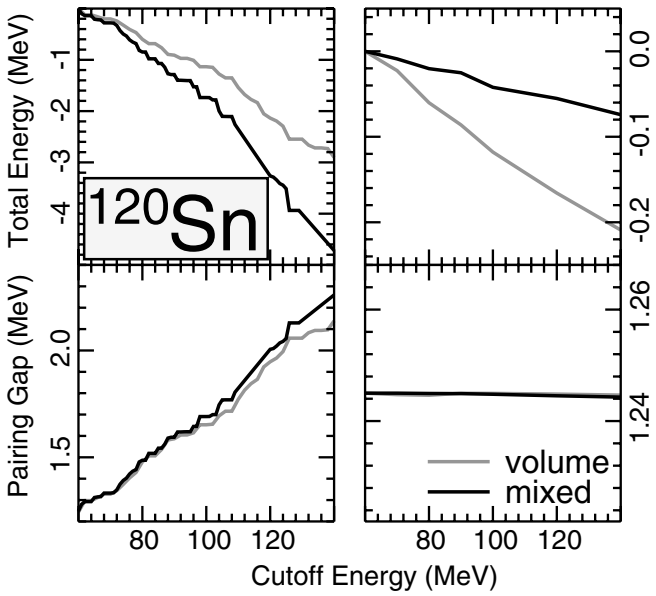

FIG. 2. Total energy (top) and neutron pairing gap (bottom) in ^{120}Sn without (left) and with (right) pairing renormalization applied. Results are shown for volume (gray) and mixed (black) pairing. Total energy is plotted relative to values obtained for cutoff energy $\epsilon_{\rm cut} =$ 60 MeV.

C. Pairing regularization

The total energy and the average neutron pairing gap in ^{120}Sn are shown in Fig. 3 after applying the pairing regularization procedure. The pairing strength V_0 is kept constant; it reproduces the neutron pairing gap for ^{120}Sn at the cutoff energy of $\epsilon_{\rm cut} =$60 MeV.

In the left panels of Fig. 3, we show results obtained in the HO basis, while the results from the solution of the HFB equations in coordinate space are displayed in the right panels.

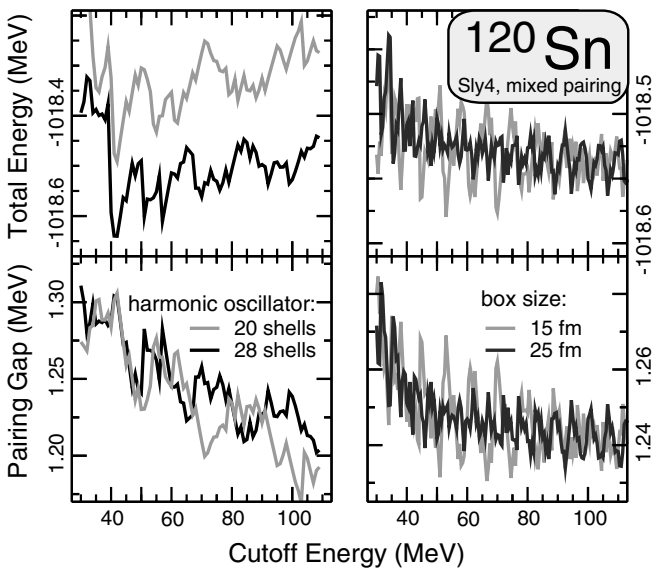

FIG. 3. Total energy (top) and neutron pairing gap (bottom) in ^{120}Sn for two values of $N_{\rm osc}$ (left) or two box sizes (right). Calculations used the mixed pairing interaction.

One can correlate the coordinate-space and HO representations by introducing an "effective box size" $R \approx \sqrt{2N_{\rm osc}\hbar/m\omega}$ [8]. Using this formula, the basis of 20 HO shells corresponds to a box radius of about 14.5 fm. Figure 3 demonstrates that the regularization procedure is stable with respect to the cutoff energy. Moreover, one obtains reasonable results already for fairly low cutoff energies of about 40 MeV. The variations in the total energy in coordinate-space calculations do not exceed 40 keV, while they are about 150 keV in the HO expansion. The latter number does not decrease significantly with $N_{\rm osc}$.

The differences in applying the pairing regularization procedure in the coordinate-space and HO calculations can be explained by the different way the quasiparticle space is expanded in both approaches. The particle density ρ is defined by the lower components of the quasiparticle wave functions, which are localized within the nuclear interior. On the other hand, the abnormal density is defined by the products of the upper and lower components of the quasiparticle wave function. For the quasiparticle energies that are greater than the modulus of the chemical potential, the upper components of the quasiparticle wave function are not localized. Therefore, contrary to the normal density, the abnormal density strongly depends on the completeness of the s.p. basis outside the nuclear interior.

In the coordinate-space calculations, the box boundary conditions provide discretization of the spectrum for the quasiparticle continuum states that are not localized. On the other hand, all the HO basis states are localized. Results of stability with respect to the cutoff energy for the coordinate-space and HO calculations are, therefore, different. As far as the description of nonlocalized states is concerned, the coordinate-space method is superior to the HO expansion method.

Fluctuations in the total energy shown in Fig. 3 coincide with $2j+1$-folded degenerate angular-momentum multiplets of states in spherical nuclei that enter the pairing window with increasing cutoff energy. This can be confirmed by performing a similar analysis for a deformed nucleus where the magnetic degeneracy is lifted. Such results are shown in Fig. 4 for deformed ^{110}Zr in comparison with spherical ^{120}Sn. One can see that the fluctuations of the total energy in ^{110}Zr are down to about 40 keV.

The steep increase in total energy at the cutoff energies below 30 MeV results from neglecting quasiparticle states with significant occupation probability. This effect is more severe for mixed pairing than for volume pairing calculations because of the surface-peaked character of mixed pairing fields. On the other hand, the stability with respect to the cutoff energy is similar in both cases.

We also tested the importance of the rearrangement terms arising as a result of the regularization procedure. The gray lines in Fig. 4 show results obtained without taking into account the second and third term of Eq. (2.12). These terms lead to changes in the total energy of a few keV and can be safely neglected.

Finally, we tested the Thomas-Fermi approximation used in the pairing regularization procedure. Instead of adopting the Thomas-Fermi ansatz, one can perform regularization using

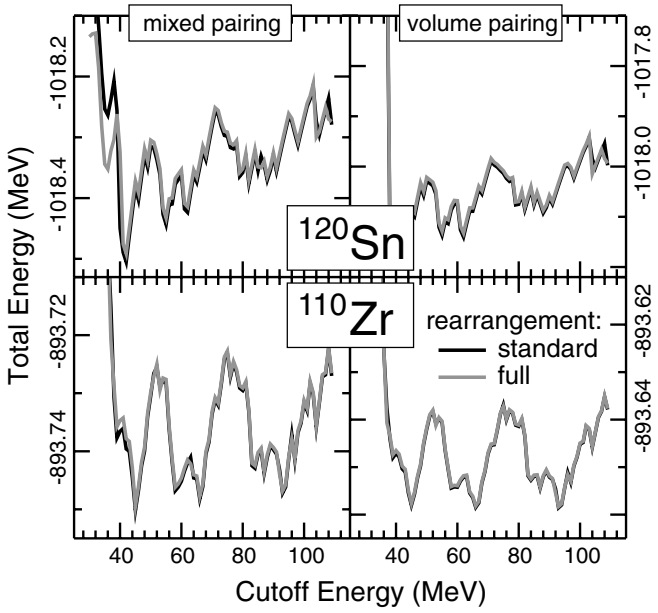

FIG. 4. Total energy of spherical ^{120}Sn (top) and deformed ^{110}Zr (bottom) obtained with pairing regularization (black lines) for mixed pairing (left) and volume pairing (right). Results obtained without the rearrangement terms from the variation of $k_{\rm cut}$ and k_F in Eq. (2.12) are also shown (gray lines).

the free particle Green's function [13]. As illustrated in Fig. 5, the convergence of the latter method is very slow; the Thomas-Fermi method is clearly superior.

D. A link between the pairing renormalization and regularization procedures

The renormalized and regularized pairing calculations are based, in fact, on two different effective interactions. Consequently, their results should be comparable only as much as their effective pairing strengths $g_{\rm eff}$ are similar. By expanding Eq. (2.11) at very high cutoff energies ($k_F/k_{\rm cut} \ll 1$), one obtains

$$g_{\rm eff}(\mathbf{r}) \approx \left(1 - \frac{M^*(\mathbf{r})g(\mathbf{r})}{2\pi^2\hbar^2}k_{\rm cut}(\mathbf{r})\right)^{-1} g(\mathbf{r}), \qquad (3.2)$$

which has the form of $g_{\rm eff} = \alpha g$. For the volume pairing, the proportionality factor α is ρ dependent only through the weak density dependence of the effective mass M^*. On the other hand, for the mixed pairing, it also depends on ρ through the density dependence of g. Therefore, while for volume pairing the renormalization procedure may be considered as a fair approximation to the regularization scheme, this is not the case for mixed pairing or – more generally – for any density-dependent pairing. Still, this approximate equality of the effective pairing strengths for the pairing regularization and renormalization explains the remarkable stability of the total energy in phenomenological pairing renormalization treatment (see Fig. 2), and it also explains why results obtained for volume pairing are more stable than those in the mixed pairing variant.

This effect can be clearly seen in Fig. 6. The ratio between the effective pairing strengths in the regularization and renormalization methods is much closer to unity for volume pairing than for mixed pairing in the region of space where the pairing energy density is maximal.

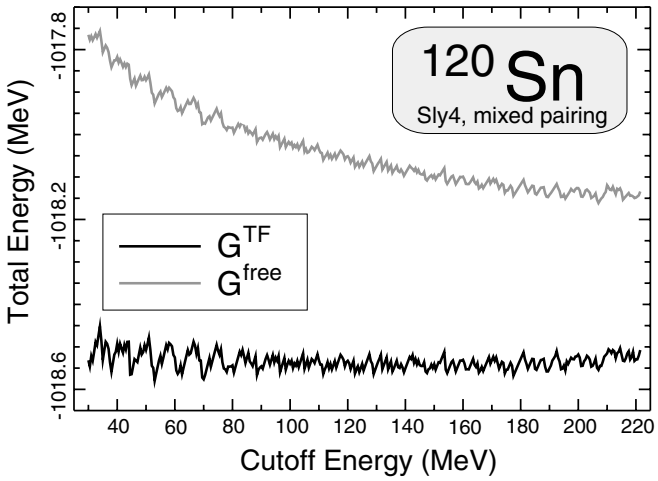

FIG. 5. Two pairing regularization schemes applied to the case of ^{120}Sn: the Thomas-Fermi approximation [19] (black line) and the free particle Green's function [13] (gray line). Coordinate-space calculations were performed in a 15 fm box.

IV. COMPARISON BETWEEN PAIRING RENORMALIZATION AND REGULARIZATION PROCEDURES

In this section, we present a comparison between pairing renormalization and regularization procedures applied to a large number of nuclei. As representative results, we discuss those obtained for the drip-to-drip line isotopic chains of spherical Sn nuclei as well as for deformed Dy nuclei.

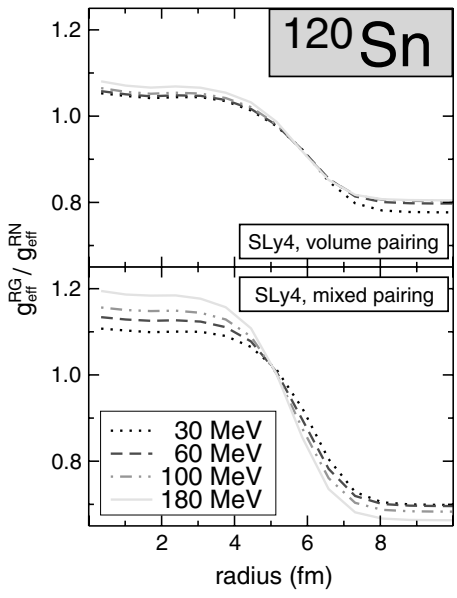

FIG. 6. Ratio between effective pairing strengths for pairing regularization and renormalization, $g_{\rm eff}^{\rm RG}/g_{\rm eff}^{\rm RN}$, for volume (upper panel) and mixed (lower panel) pairing in ^{120}Sn for several values of $\epsilon_{\rm cut}$.

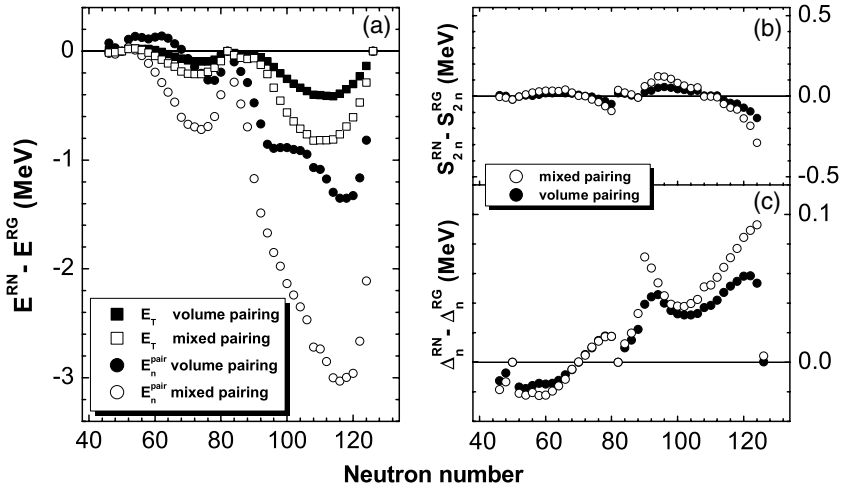

FIG. 7. Differences between pairing renormalization (RN) and regularization (RG) procedures for (a) total and neutron pairing energies, (b) two-neutron separation energies, and (c) average neutron gaps. The HFB+THO calculations were performed for the spherical Sn isotope chain using the SkP Skyrme parametrization.

Calculations are performed for volume and/or mixed pairing interactions by using the HFB+THO approach. The isotopic chains include all particle-bound even-even nuclei, including the drip line systems. The stability of the regularization procedure is primarily determined by equivalent energies around the cutoff energy. Therefore, the quality of results is comparable for stable nuclei and weakly bound systems.

A. Spherical nuclei

Figure 7 displays differences between the pairing renormalization and regularization procedures for the Sn isotopes. Calculations are performed with both volume and mixed pairing interactions. For the two-neutron separation energies, the maximum difference between the renormalization and regularization schemes is about 100 (300) keV for the volume (mixed) pairing. In the neutron gap, the corresponding difference is about 50 (100) keV, and in nuclear radii (not displayed) it is practically negligible (about 0.01 fm). The largest differences show up in pairing energies—about 1 (3) MeV for the volume (mixed) pairing. However, total energy differences are much smaller—about 400 (800) keV.

Analyzing the total energies obtained in both methods, in Fig. 7(a), one can see that the pairing renormalization procedure gives systematically more binding. The differences are negligible for stable nuclei and nuclei near the proton drip line. They increase in midshell nuclei near the two-neutron drip line where the pairing effects are the largest, and then decrease toward the closed-shell nucleus ^{176}Sn located just at the two-neutron drip line. In general, both procedures give more similar results in the case of volume pairing than in the case of mixed pairing.

Recently, the pairing regularization procedure has been analyzed in the context of relativistic mean-field approximation [24]. In order to simulate the finite-range contribution to the nuclear matter pairing gap coming from the Gogny pairing force, it was necessary to introduce strong density dependence in the pairing strength of the contact interaction.

Using the regularization procedure and calculating the Sn chain with both volume and newly constructed (surface)

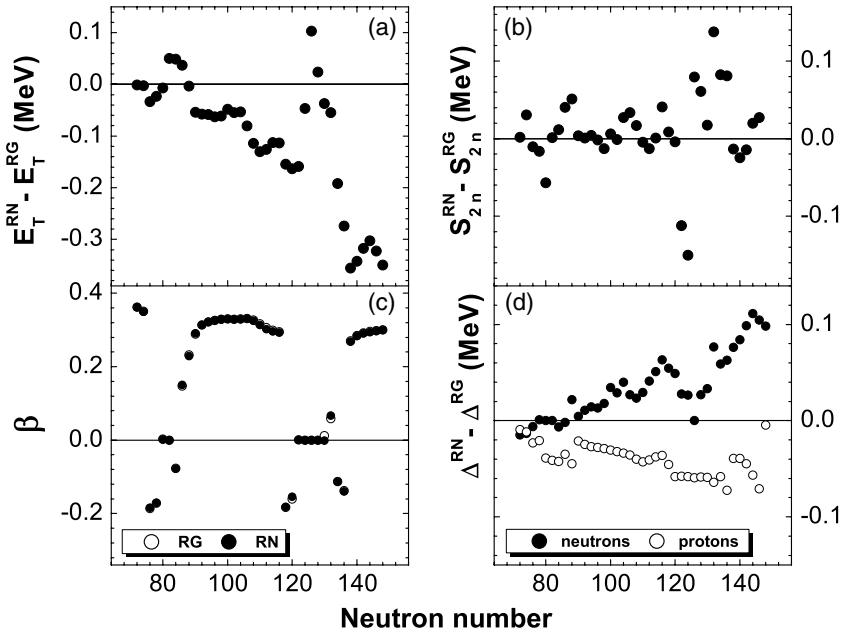

FIG. 8. Similar to Fig. 7, but for deformed Dy isotopes. Quadrupole deformations are displayed in panel (c). Mixed pairing interaction was used.

contact interaction, the authors of Ref. [24] found differences in pairing energies of the order of 20 MeV in the neutron-rich nuclei around ^{148}Sn. In our work, for the same nuclei, the differences in pairing energies between volume and mixed pairing variants do not exceed 2.6 MeV. This comparison shows that the density-dependent contact interaction proposed in Ref. [24] is questionable for finite nuclei, despite its agreement with the finite-range Gogny pairing force in the infinite nuclear matter.

B. Deformed nuclei

We applied the pairing renormalization and regularization procedures to the chain of deformed Dy isotopes. Differences between both sets of results are shown in Fig. 8. We show only the results with mixed pairing, since, as in the spherical nuclei, the differences between both procedures are larger in this case.

As seen in Fig. 8(c), most of the nuclei considered are well deformed, and the deformations are practically the same within both procedures. Despite the fact that the maximum difference in the pairing energy is around 3 MeV (not shown), other quantities are very similar. The maximum difference in the total energy is about 360 keV; in the two-neutron separation energy, 160 keV; in the pairing gaps, 110 keV; and in the rms radii (not shown), less than 0.005 fm.

V. SUMMARY AND CONCLUSIONS

In this work, we investigated the pairing regularization method using the s.p. Green's function in the Thomas-Fermi approximation and found it to be very suitable for describing spherical and deformed nuclei. We checked the stability of the method with respect to the cutoff energy and found fluctuations in the total energy below 200 keV. Fluctuations coming from the method itself do not exceed 50 keV for the cutoff energy as low as 30 MeV. However, if a still lower cutoff energy is assumed, the Thomas-Fermi approximation to the s.p. Green's function may no longer be valid.

We found that the differences between pairing renormalization and regularization procedures for volume and mixed pairing are rather small. Therefore, we conclude that physical conclusions previously obtained within the pairing renormalization scheme remain valid. Nevertheless, we believe that the theoretical motivation and simplicity of the regularization method is preferred to a phenomenological renormalization scheme.

ACKNOWLEDGMENTS

Discussions with Aurel Bulgac are gratefully acknowledged. This work was supported in part by the U.S. Department of Energy under Contract Nos. DE-FG02-96ER40963 (University of Tennessee) and DE-AC05-00OR22725 with UT-Battelle, LLC (Oak Ridge National Laboratory), by the National Nuclear Security Administration under the Stewardship Science Academic Alliances program through DOE Research Grant DE-FG03-03NA00083, by the Polish Committee for Scientific Research (KBN) under Contract No. 1 P03B 059 27, and by the Foundation for Polish Science (FNP).

APPENDIX: DIVERGENCE IN ABNORMAL DENSITY

In the DFT-HFB approach, the starting point is the energy density functional (EDF) $\mathcal{H}[\rho, \tilde{\rho}]$, where ρ is the particle density and $\tilde{\rho}$ is the abnormal density

$$\rho(\mathbf{r_2}\sigma_2\tau_2, \mathbf{r_1}\sigma_1\tau_1) = \langle\Phi|a^\dagger_{\mathbf{r_1}\sigma_1\tau_1} a_{\mathbf{r_2}\sigma_2\tau_2}|\Phi\rangle, \tag{A1}$$

$$\tilde{\rho}(\mathbf{r_2}\sigma_2\tau_2, \mathbf{r_1}\sigma_1\tau_1) = -2\sigma_1\langle\Phi|a_{\mathbf{r_1}-\sigma_1\tau_1} a_{\mathbf{r_2}\sigma_2\tau_2}|\Phi\rangle, \tag{A2}$$

where a and $a^\dagger$ are the particle annihilation and creation operators, respectively, and $|\Phi\rangle$ is the HFB state. In the following, we assume that $|\Phi\rangle$ is a product of the neutron and proton states, $|\Phi_\nu\rangle|\Phi_\pi\rangle$. Therefore, the neutron and proton wave functions are not coupled, and in the notation below we can, for simplicity, omit the isospin index with the understanding that all equations are separately valid for neutrons and protons.

For the HFB state $|\Phi\rangle$, the particle and abnormal densities can be written as [12]

$$\rho(\mathbf{r_2}\sigma_2, \mathbf{r_1}\sigma_1) = \sum_{E_i>0} \varphi_{2i}(\mathbf{r_2}\sigma_2)\varphi^*_{2i}(\mathbf{r_1}\sigma_1), \tag{A3}$$

$$\tilde{\rho}(\mathbf{r_2}\sigma_2, \mathbf{r_1}\sigma_1) = -\sum_{E_i>0} \varphi_{2i}(\mathbf{r_2}\sigma_2)\varphi^*_{1i}(\mathbf{r_1}\sigma_1), \tag{A4}$$

where the two-component quasiparticle wave function φ is the solution of the HFB equation

$$\sum_{\sigma_1}\int d^3\mathbf{r_1} \begin{bmatrix} h_\mu(\mathbf{r_2}\sigma_2, \mathbf{r_1}\sigma_1) & \tilde{h}(\mathbf{r_2}\sigma_2, \mathbf{r_1}\sigma_1) \\ \tilde{h}(\mathbf{r_2}\sigma_2, \mathbf{r_1}\sigma_1) & -h_\mu(\mathbf{r_2}\sigma_2, \mathbf{r_1}\sigma_1) \end{bmatrix} \times \begin{bmatrix} \varphi_{1i}(\mathbf{r_1}\sigma_1) \\ \varphi_{2i}(\mathbf{r_1}\sigma_1) \end{bmatrix} = E_i \begin{bmatrix} \varphi_{1i}(\mathbf{r_2}\sigma_2) \\ \varphi_{2i}(\mathbf{r_2}\sigma_2) \end{bmatrix}, \tag{A5}$$

for a given quasiparticle energy E_i.

The HFB equations are a result of variational minimization of the energy density functional $\mathcal{H}[\rho, \tilde{\rho}]$ with the constraint of the mean value of particles kept constant:

$$\delta\mathcal{H}|_{\langle\hat{N}\rangle=N} = 0. \tag{A6}$$

This condition defines the s.p. Hamiltonian h_μ and the pairing Hamiltonian $\tilde{h}$ in the HFB equations (A5) as

$$\begin{aligned} h_\mu(\mathbf{r_2}\sigma_2, \mathbf{r_1}\sigma_1) &= \frac{\delta\mathcal{H}[\rho, \tilde{\rho}]}{\delta\rho(\mathbf{r_1}\sigma_1, \mathbf{r_2}\sigma_2)} - \mu \\ &= -\nabla_{\mathbf{r_2}} \frac{\hbar^2}{2M^*(\mathbf{r_2}\sigma_2, \mathbf{r_1}\sigma_1)} \nabla_{\mathbf{r_1}} \\ &\quad + U(\mathbf{r_2}\sigma_2, \mathbf{r_1}\sigma_1) - \mu, \end{aligned} \tag{A7}$$

$$\tilde{h}(\mathbf{r_2}\sigma_2, \mathbf{r_1}\sigma_1) = \frac{\delta\mathcal{H}[\rho, \tilde{\rho}]}{\delta\tilde{\rho}(\mathbf{r_1}\sigma_2, \mathbf{r_2}\sigma_2)}, \tag{A8}$$

where M^* is the effective mass and U is the self-consistent mean-field potential. In the following derivations, the spin-orbit term is omitted as unimportant in the regularization scheme, although it is, of course, always included in calculations.

By multiplying the HFB equations (A5) by vector $[\varphi^*_{2i}, -\varphi^*_{1i}]$, integrating over coordinates, and summing over

all the positive energy HFB solutions, one obtains

$$\sum_{E_i>0,\sigma_2} E_i \int d^3\mathbf{r_2}\left[\varphi^*_{2i}(\mathbf{r_2}\sigma_2),\ -\varphi^*_{1i}(\mathbf{r_2}\sigma_2)\right]\begin{bmatrix}\varphi_{1i}(\mathbf{r_2}\sigma_2)\\ \varphi_{2i}(\mathbf{r_2}\sigma_2)\end{bmatrix}$$
$$= \sum_{E_i>0,\sigma_1\sigma_2}\iint d^3\mathbf{r_1}d^3\mathbf{r_2}\left[\varphi^*_{2i}(\mathbf{r_2}\sigma_2),\ -\varphi^*_{1i}(\mathbf{r_2}\sigma_2)\right]$$
$$\times\begin{bmatrix}h_\mu(\mathbf{r_2}\sigma_2,\mathbf{r_1}\sigma_1) & \tilde h(\mathbf{r_2}\sigma_2,\mathbf{r_1}\sigma_1)\\ \tilde h(\mathbf{r_2}\sigma_2,\mathbf{r_1}\sigma_1) & -h_\mu(\mathbf{r_2}\sigma_2,\mathbf{r_1}\sigma_1)\end{bmatrix}\begin{bmatrix}\varphi_{1i}(\mathbf{r_1}\sigma_1)\\ \varphi_{2i}(\mathbf{r_1}\sigma_1)\end{bmatrix} \quad \text{(A9)}$$

i.e.,

$$\sum_{E_i>0,\sigma_1} E_i\int d^3\mathbf{r_1}\{\varphi^*_{2i}(\mathbf{r_1}\sigma_1)\varphi_{1i}(\mathbf{r_1}\sigma_1)-\varphi^*_{1i}(\mathbf{r_1}\sigma_1)\varphi_{2i}(\mathbf{r_1}\sigma_1)\}$$
$$= \sum_{E_i>0,\sigma_1\sigma_2}\iint d^3\mathbf{r_1}d^3\mathbf{r_2}\{\varphi^*_{2i}(\mathbf{r_2}\sigma_2)h_\mu(\mathbf{r_2}\sigma_2,\mathbf{r_1}\sigma_1)\varphi_{1i}(\mathbf{r_1}\sigma_1)$$
$$+\varphi^*_{2i}(\mathbf{r_2}\sigma_2)\tilde h(\mathbf{r_2}\sigma_2,\mathbf{r_1}\sigma_1)\varphi_{2i}(\mathbf{r_1}\sigma_1)$$
$$+\varphi^*_{1i}(\mathbf{r_2}\sigma_2)h_\mu(\mathbf{r_2}\sigma_2,\mathbf{r_1}\sigma_1)\varphi_{2i}(\mathbf{r_1}\sigma_1)$$
$$-\varphi^*_{1i}(\mathbf{r_2}\sigma_2)\tilde h(\mathbf{r_2}\sigma_2,\mathbf{r_1}\sigma_1)\varphi_{1i}(\mathbf{r_1}\sigma_1)\}. \quad \text{(A10)}$$

Since for every HFB solution $([\varphi_{1i},\varphi_{2i}],E_i)$ there exists also an orthogonal solution $([\varphi_{2i},-\varphi_{1i}],-E_i)$, the left-hand side of Eq. (A10) vanishes as a sum over scalar products of orthogonal wave functions.

For local and spin-independent Hamiltonians h_μ and $\tilde h$, Eqs. (A7) and (A8) read

$$h_\mu(\mathbf{r_2}\sigma_2,\mathbf{r_1}\sigma_1) = -\nabla_{\mathbf{r_2}}\frac{\hbar^2}{2M^*(\mathbf{r_2})}\delta(\mathbf{r_2}-\mathbf{r_1})\delta_{\sigma_2,\sigma_1}\nabla_{\mathbf{r_1}} + (U(\mathbf{r_2})-\mu)\delta(\mathbf{r_2}-\mathbf{r_1})\delta_{\sigma_2,\sigma_1}, \quad \text{(A11)}$$

$$\tilde h(\mathbf{r_2}\sigma_2,\mathbf{r_1}\sigma_1) = \tilde h(\mathbf{r_2})\delta(\mathbf{r_2}-\mathbf{r_1})\delta_{\sigma_2,\sigma_1}. \quad \text{(A12)}$$

Note that for an attractive pairing force, the local pairing potential $\tilde h(\mathbf{r}) = -\Delta(\mathbf{r})$ is negative, where $\Delta(\mathbf{r})$ is the standard position-dependent pairing gap. By defining function $\mathcal{F}_{\epsilon_{\rm cut}}$ as

$$\sum_{E_i>0,\sigma}[\varphi_{1i}(\mathbf{r_2}\sigma)\varphi^*_{1i}(\mathbf{r_1}\sigma)+\varphi_{2i}(\mathbf{r_2}\sigma)\varphi^*_{2i}(\mathbf{r_1}\sigma)] = \mathcal{F}_{\epsilon_{\rm cut}}(\mathbf{r_2}-\mathbf{r_1}) \quad \text{(A13)}$$

and using expression (A4) for the abnormal density, one obtains after integrating the kinetic energy term by parts

$$0 = -\int d^3\mathbf{r_1}d^3\mathbf{r_2}\delta(\mathbf{r_2}-\mathbf{r_1})\Big[\tilde h(\mathbf{r_2})[\mathcal{F}_{\epsilon_{\rm cut}}(\mathbf{r_2}-\mathbf{r_1}) - 2\rho(\mathbf{r_2},\mathbf{r_1})] + \left(\frac{\hbar^2}{2M^*}\nabla_{\mathbf{r_2}}\nabla_{\mathbf{r_1}}+U(\mathbf{r_2})-\mu\right)2\tilde\rho(\mathbf{r_1},\mathbf{r_2})\Big]$$
$$= -\int d^3\mathbf{r}d^3\mathbf{x}\delta(\mathbf{x})\Big[\tilde h(\mathbf{r})[\mathcal{F}_{\epsilon_{\rm cut}}(\mathbf{x})-2\rho(\mathbf{r},\mathbf{r})] + \left(\frac{\hbar^2}{2M^*}\left(\frac{1}{4}\nabla^2_{\mathbf{r}}-\nabla^2_{\mathbf{x}}\right)+U(\mathbf{r})-\mu\right) \times 2\tilde\rho(\mathbf{r}-\mathbf{x}/2,\mathbf{r}+\mathbf{x}/2)\Big], \quad \text{(A14)}$$

where

$$\mathbf{r} = \frac{\mathbf{r_1}+\mathbf{r_2}}{2}, \quad \text{(A15)}$$

$$\mathbf{x} = \mathbf{r_2}-\mathbf{r_1}, \quad \text{(A16)}$$

and

$$\rho(\mathbf{r_2},\mathbf{r_1}) = \sum_\sigma \rho(\mathbf{r_2}\sigma,\mathbf{r_1}\sigma), \quad \text{(A17)}$$

$$\tilde\rho(\mathbf{r_2},\mathbf{r_1}) = \sum_\sigma \tilde\rho(\mathbf{r_2}\sigma,\mathbf{r_1}\sigma). \quad \text{(A18)}$$

When the summation over positive quasiparticle energies is extended to infinity, the completeness relation implies that

$$\mathcal{F}_{\epsilon_{\rm cut}}(\mathbf{r_2}-\mathbf{r_1}) = \delta(\mathbf{r_2}-\mathbf{r_1}), \quad \text{(A19)}$$

and the only term in Eq. (A14) capable of canceling out this singularity is $\nabla^2_{\mathbf{x}}\tilde\rho(\mathbf{r}-\mathbf{x}/2,\mathbf{r}+\mathbf{x}/2)$. Therefore, the Laplacian of the abnormal density $\nabla^2_{\mathbf{x}}\tilde\rho(\mathbf{r}-\mathbf{x}/2,\mathbf{r}+\mathbf{x}/2)$ must be singular at $\mathbf{x}=0$. Moreover, using the expression

$$\nabla^2\frac{1}{|\mathbf{r}|} = -4\pi\delta(\mathbf{r}), \quad \text{(A20)}$$

it is clear that because of the zero-range pairing interaction, abnormal density $\tilde\rho$ has an ultraviolet $1/x$ divergence:

$$\tilde\rho(\mathbf{r}-\mathbf{x}/2,\mathbf{r}+\mathbf{x}/2) \sim -\frac{\tilde h(\mathbf{r})M^*(\mathbf{r})}{4\pi\hbar^2|\mathbf{x}|}\bigg|_{\mathbf{x}\to 0}. \quad \text{(A21)}$$

[1] P. Hohenberg and W. Kohn, Phys. Rev. **136**, B864 (1964).
[2] W. Kohn and L. J. Sham, Phys. Rev. **140**, A1133 (1965).
[3] T. H. R. Skyrme, Phil. Mag. **1**, 1043 (1956).
[4] D. Vauterin and D. M Brink, Phys. Rev. C **5**, 626 (1972).
[5] E. Perlińska, S. G. Rohozinski, J. Dobaczewski, and W. Nazarewicz, Phys. Rev. C **69**, 014316 (2004).
[6] M. Samyn, S. Goriely, P.-H. Heenen, J. M. Pearson, and F. Tondeur, Nucl. Phys. **A700**, 142 (2002).
[7] S. Goriely, M. Samyn, P.-H. Heenen, J. M. Pearson, and F. Tondeur, Phys. Rev. C **66**, 024326 (2002).
[8] J. Dobaczewski, W. Nazarewicz, T. R. Werner, J. F. Berger, C. R. Chinn, and J. Dechargé, Phys. Rev. C **53**, 2809 (1996).
[9] J. Dobaczewski, W. Nazarewicz, and P.-G. Reinhard, Nucl. Phys. **A693**, 361 (2001).
[10] J. Dechargé and D. Gogny, Phys. Rev. C **21**, 1568 (1980).
[11] R. R. Chasman, Phys. Rev. C **14**, 1935 (1976).
[12] J. Dobaczewski, H. Flocard, and J. Treiner, Nucl. Phys. **A422**, 103 (1984).
[13] H. Esbensen, G. F. Bertsch, and K. Hencken, Phys. Rev. C **56**, 3054 (1997).
[14] M. Marini, F. Pistolesi, and G. C. Strinati, Eur. Phys. J. B **1**, 151 (1998).
[15] T. Papenbrock and G. F. Bertsch, Phys. Rev. C **59**, 2052 (1999).
[16] G. Bruun, Y. Castin, R. Dum, and K. Burnett, Eur. Phys. J. D **7**, 433 (1999).

[17] A. Bulgac, nucl-th/9907088.
[18] A. Bulgac and Y. Yu, nucl-th/0109083.
[19] A. Bulgac and Y. Yu, Phys. Rev. Lett. **88**, 042504 (2002).
[20] A. Bulgac, Phys. Rev. C **65**, 051305(R) (2002).
[21] Y. Yu and A. Bulgac, Phys. Rev. Lett. **90**, 222501 (2003).
[22] A. Bulgac and Y. Yu, Int. J. Mod. Phys. E **13**, 147 (2004).
[23] T. Duguet, K. Bennaceur, and P. Bonche, nucl-th/0508054, in *Proceedings of the YITP Workshop on New Developments in Nuclear Self-Consistent Mean-Field Theories, Kyoto, 2005* (YITP-W-05-01), p. B20.
[24] T. Nikšić, P. Ring, and D. Vretenar, Phys. Rev. C **71**, 044320 (2005).
[25] M. Grasso and M. Urban, Phys. Rev. A **68**, 033610 (2003).
[26] P. Ring and P. Schuck, *The Nuclear Many-Body Problem* (Springer-Verlag, New York, 1980).
[27] M. V. Stoitsov, J. Dobaczewski, W. Nazarewicz, and P. Ring, Comput. Phys. Commun. **167**, 43 (2005).
[28] K. Bennaceur and J. Dobaczewski, Comput. Phys. Commun. **168**, 96 (2005).
[29] E. Chabanat, P. Bonche, P. Haensel, J. Meyer, and F. Schaeffer, Nucl. Phys. **A635**, 231 (1998).
[30] J. Dobaczewski, W. Nazarewicz, and M. V. Stoitsov, Eur. Phys. J. A **15**, 21 (2002).